ELSEVIER

Chemical Engineering Journal 71 (1998) 243–252

Chemical Engineering Journal

# The role of thermal and transport properties on the binder burnout of injection-molded ceramic components

Alan C. West[a], Stephen J. Lombardo[1,b,*]

[a] *Department of Chemical Engineering, Columbia University, New York, NY 10027, USA*

[b] *Northboro Research and Development Center, Saint-Gobain Norton Industrial Ceramics, Goddard Road, Northboro, MA 01532, USA*

Received 16 December 1997; received in revised form 30 March 1998; accepted 14 April 1998

**Abstract**

A mathematical model is developed for describing the decomposition and removal of binder from ceramic components formed by injection molding. The model takes into account heat transfer by conduction within the ceramic body, mass transfer by convective flow of gas products, and an Arrhenius dependence of the decomposition rate. The model is solved numerically to determine the spatial and temporal evolution of temperature, reaction rate, concentration, porosity, and pressure. The influences of the thermal and transport properties on the distribution of binder and on the buildup of pressure within the body are examined. When small temperature gradients exist across the body, the binder is removed homogenously, whereas when large temperature gradients are present, the binder is removed as a receding planar front. 

*Keywords:* Injection molded ceramic components; Thermal and transport properties; Binder burnout

## 1. Introduction

Injection molding as a forming technology offers a number of advantages for the manufacture of ceramic components [1–3]. The rapidity of production coupled with superior surface finish and the ability to maintain dimensional tolerances makes injection molding one of the most promising forming techniques for high volume, complex ceramic shapes. In spite of these advantages, the problems associated with the removal of the binder used to convey the ceramic particulates into the mold have impeded the wide utilization of this forming method.

During binder burnout, a number of physical phenomena can occur which can degrade and ultimately lead to the rejection of the ceramic components. These include slumping of the body, at the surface, and cracking within the body. To a large extent, these defects arise due to phase changes of the binder and mass-transfer limitations during the binder removal step.

From a mechanistic viewpoint, the thermal decomposition of binder and its removal from the green body arise as a consequence of the coupling between heat transfer, mass transfer, and reaction kinetics. In a typical burnout cycle in which the temperature of the furnace is slowly ramped in time, temperature gradients occur within the body and spatial variation in the decomposition rate develop. Since the decomposition of the binder is position dependent, gradients in binder concentration are found within the pore space of the body. The spatial dependence of the decomposition rate of the binder also leads to pressure gradients within the body. For cases where the internal resistance of the body to flow is large, the relief of pressure is insufficiently fast, and the pressure increase can lead to fracture of the ceramic green body.

During burnout, the concentration of binder within the green body is generally assumed to be distributed in one of the two limiting cases [4–7]. In one case, binder decomposition is assumed to begin at the outer edge of the body and then to recede with time as a planar front into the body. This is referred to as planar binder removal. In the second case, binder is assumed to decompose uniformly throughout the body leaving no concentration gradients. While most of the theoretical work [4,5] has been based upon the assumption of a receding planar front, the limited experimental data [6,7] indicate that binder removal is a more homogeneous process. One focus of this work is to identify the conditions under which these two limiting cases occur.

*Corresponding author.

[1] Present address: Department of Chemical Engineering, University of Missouri, Columbia, MO 65211.

1385-8947/98/$ – see front matter 
PII: S1385-8947(98)00098-9

A number of authors [4,5,8–15] have examined theoretical aspects of the binder removal operation. Barone and Ulicny [8] treated the stress arising from thermal expansion of the binder as a function of heating rate. For heating rates of 600°C/h, the stress in a 50 : 50 mixture of wax and polyethylene can approach 2–4 atm; for heating rates of 10°C/h typically used for binder burnout from monolithic ceramics, their calculations indicate orders of magnitude lower stresses.

Tsai [9] and Manguin-Fritsch et al. [10] have developed models that take into account the effects of thermal gradients and flow within the body. Both works demonstrated that non-uniform binder and pressure distributions can occur during binder decomposition. The pressure increase within the body can be quite large and can reach 10 times the ambient pressure in the furnace. Since these works either treated the thermal and transport properties as constant or varied them over a narrow range of possible values, it was not apparent to what extent the thermal and transport properties of the system are responsible for the binder profiles and pressure increases.

The aim of this work is to develop a model for binder burnout that will show under what conditions binder removal proceeds as a planar front and under what conditions it proceeds homogeneously. The physical parameters which will be shown to control the distribution of binder are the thermal properties (thermal conductivity and heat capacity) and the transport properties (specific surface area, tortuosity, and gas viscosity). It will be shown further that these same parameters control the magnitude of the pressure increases, and hence, within the body. Finally, as an outcome of this analysis, it will be seen how the physical quantities for a given system can be used to determine instances in which inhomogeneous binder distributions and pressure effects are significant.

## 2. Theory

A comprehensive model of the removal of binder from a green body requires consideration of heat and mass-transfer phenomena as well as the kinetics of polymer degradation. The role of the thermal and transport properties is examined through consideration of the time constants characteristic of each process. The model is then solved for values of the time constants representative of the conditions likely to be found in ceramic processing. It will be seen that the range of both time constants spans three orders of magnitude. As a consequence of these large ranges, other dependences which only vary by factors of up to 2 over the temperature range of consideration (300–700 K) will not be explicitly treated. With this approach, a simple but rigorous model is developed which captures the salient features of the binder burnout process while remaining transparent enough to demonstrate cause and effect relationships.

The key assumptions in the model which account for the essential physical processes are:

1. Conduction is the only mode of heat transfer in the green body.
2. The thermal diffusivity $\alpha$ does not vary with temperature.
3. Binder burnout can be described by zero-order kinetics with an Arrhenius temperature dependence.
4. Binder decomposition products are all gas phase.
5. Darcy's law can be used to describe the gas flow of decomposition products out of the body.

Both assumptions 1 and 2 are justified in light of the preceding comments regarding the variations in the thermal and transport properties which will be treated in this work. While assumption 1 is reasonable, it should be recognized that the binder has a comparable thermal diffusivity to that of the green body. Binder removal thus has the effect of decreasing the effective thermal diffusivity of the body with time.

Assumptions 3 and 4 represent the simplest form of binder decomposition kinetics. Real binder systems for injection-molded ceramic components are often multi-component mixtures of diverse chemical origin such as waxes, oils, polymers, surfactants, etc. Depending on the particular nature of the individual species, the gas environment, the heating rate, and the catalytic effects of the ceramic powder, the binder removal may proceed as vaporization, unzipping, combustion, or pyrolysis. The multitude of possibilities precludes treating all cases; we thus treat the case described by assumptions 3 and 4.

The validity of the fifth assumption depends on the ratio of the mean free path of the gas-phase species as compared to the pore radius [9,16]. When the pore size is large relative to the mean free path of the gas-phase species, laminar flow, as described by Darcy's law, occurs. For the case when the pore size is near the value of the mean free path of the molecules, slip flow occurs, i.e., a combination of laminar and Knudsen flow. Slip flow is faster than laminar flow.

In real green bodies, however, a pore size distribution exists in which the nature of the flow process depends upon the local ratio of the mean free path to pore radius. In keeping with the approach adapted here, we only consider the case of the slower transport process, namely laminar flow, and thus determine the upper bound on pressure increases. It is this bound which is important in designing a temperature cycle for binder removal which minimizes stresses within the body.

### 2.1. Temperature variations

Since conduction is the only mode of heat transfer operative at the conditions treated here, the temperature, $T$, as a function of position and time, $t$, is given by

$$\frac{\partial T}{\partial t} = \alpha \frac{\partial^2 T}{\partial x^2} \tag{1}$$

subject to the initial condition

$$\text{at } t = 0 \quad T = T_0 \tag{2}$$

where $x$ represents the spatial coordinate, $\alpha$ the thermal diffusivity, and $T_0$ the initial temperature. Implicit in the formulation of Eq. (1) is that the heat of reaction and convective heat transfer within the body are negligible. For the case where the heat-transfer resistance between the body and the furnace wall is small, the boundary conditions at the edges of the body are given by

$$\text{at } x = \pm L, \quad T = T_0 + \sigma t \tag{3}$$

where $L$ is the half-thickness of the body and $\sigma$ is the rate at which the temperature in the furnace is being ramped. Symmetry permits the condition at $x = -L$ to be replaced with

$$\text{at } x = 0, \quad \frac{\partial T}{\partial x} = 0 \tag{4}$$

A schematic of the green body and the appropriate boundary conditions for the temperature profile and pressure distribution, discussed below, are shown in Fig. 1

Carslaw and Jaeger [17] provide an analytical solution to Eqs. (1)–(4) as

$$T - T_0 = \frac{\sigma L^2}{\alpha}\Theta(\bar{x}, \tau) \tag{5}$$

where $\bar{x} = x/L$ is a dimensionless distance and $\tau = (\alpha t)/(L^2)$ is a dimensionless time. The function $\Theta$ is given by

$$\Theta(\bar{x}, \tau) = \tau + \frac{\bar{x}^2 - 1}{2} + \frac{16}{\pi^3}\sum_{n=0}^{\infty}\frac{(-1)^n}{(2n+1)^3}\exp(-\lambda_n^2\tau)\cos(\lambda_n\bar{x}) \tag{6}$$

with $\lambda_n = (2n + 1)\pi/2$.

Eq. (5) shows that the maximum temperature difference within the body scales with $\sigma L^2/\alpha$. The spatial variation of the temperature as a function of time can most easily be seen

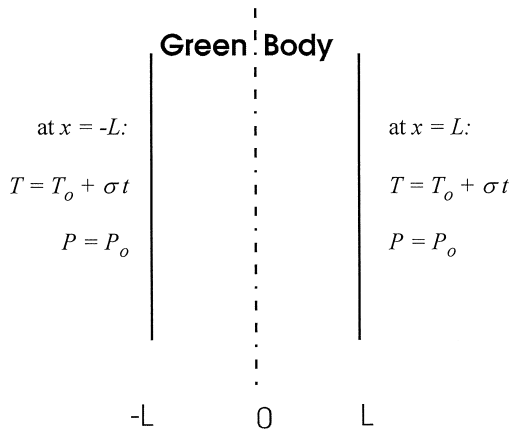


Fig. 1. Schematic of the one-dimensional model of a green body. At the body edges ($x = \pm L$), the temperature and pressure are given by the conditions in the furnace.

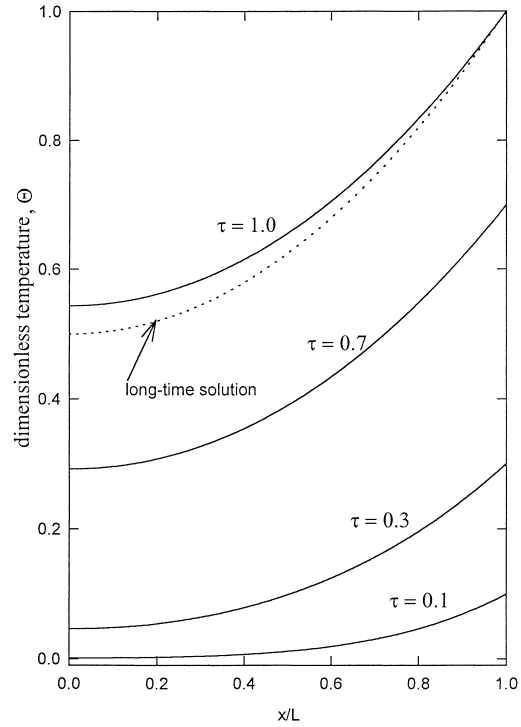


Fig. 2. The dimensionless temperature $\Theta$ vs. position within the body for four values of the dimensionless time $\tau$. The dotted line is the long-time solution (see Eq. (7)) for $\tau = 1.0$

by examining $\Theta$; this is shown in Fig. 2 for four dimensionless times, $\tau$. For short times, i.e., small $\tau$, the temperature gradient across the body is small and becomes more pronounced for larger values of $\tau$. The dashed line for $\tau = 1$ represents the long-time solution obtained by neglecting all the terms in the series:

$$T - T_0 = \frac{\sigma L^2}{\alpha}\left(\tau + \frac{\bar{x}^2 - 1}{2}\right) \quad \text{for large } \tau \tag{7}$$

For approximately $\tau \geq 4$, the long-time solution is nearly indistinguishable from the full solution.

### 2.2. Binder burnout kinetics

The decomposition rate $r$ of binder is based upon the Arrhenius relationship of Cima et al. [5]:

$$r = k_0\exp\left(-\frac{E_a}{RT}\right) \tag{8}$$

where $k_0 = 3.87 \times 10^{14}$ kg/m$^3$/s and $E_a = 17500$ Joules/mole. For these values of the kinetic parameters, the reaction rate is very slow at temperatures below 500 K. Above this temperature, the reaction rate increases quickly according to the exponential dependence.

### 2.3. Porosity creation

The volume fraction of binder $V_b$ within the body decreases with time and can be determined from conserva-

tion of mass. For a constant density of polymer $\rho_b$, the change in volume fraction of binder is proportional to the reaction rate:

$$V_b(x,t) = V_{b,0} - \int_0^t \frac{r(x,t)}{\rho_b}\,dt \tag{9}$$

where $V_{b,0}$ is the initial volume fraction of binder $V_b$ is known from Eq. (9), the volume fraction of the body occupied by gas is given by

$$V_g = 1 - V_s - V_b \tag{10}$$

where $V_s$ is the volume fraction of ceramic in the green body, taken to be 0.6 in the simulations presented here.

### 2.4. Pressure increase

Due to the evolution of gas-phase products produced by polymer decomposition, the pressure increases within the body. To alleviate the pressure increase, gas flows out of the body. The continuity equation applied to the gas phase can be written as

$$\frac{\partial(V_g\rho)}{\partial t} = -\frac{\partial}{\partial x}(\rho u) + \frac{r(x,t)}{M} \tag{11}$$

where $\rho$ is taken to be the molar gas density, and $M$ is the average molecular weight of the gas-phase products. The superficial velocity $u$ can be given by Darcy's law [13,14,18]

$$u = -\frac{\kappa}{\mu}\frac{\partial p}{\partial x} \tag{12}$$

where $\mu$ is the viscosity of the gas. The gas permeability $\kappa$ appearing in Eq. (12) is most simply represented by the Kozeny–Carman form [13,18]

$$\kappa = \frac{V_g^3}{k(1-V_g)^2 S^2} \tag{13}$$

where $k$ – typically between 3 and 7 – is a constant accounting for the shape of the pores, and $S$ is the surface area per unit volume of the body [13,18,19].

Combining Eqs. (11)–(13), as well as assuming an ideal gas (i.e., $p = \rho RT$) gives

$$\frac{\partial(V_g\rho)}{\partial t} = \beta_1(x,t)\left[\rho\frac{\partial^2\rho}{\partial x^2} + \left(\frac{\partial\rho}{\partial x}\right)^2\right] + \beta_2(x,t)\rho\frac{\partial\rho}{\partial x} + \beta_3(x,t)\rho^2 + \frac{r(x,t)}{M} \tag{14}$$

where

$$\beta_1(x,t) = \frac{\kappa RT}{\mu} \tag{15}$$

$$\beta_2(x,t) = R\left(\frac{3\kappa}{\mu}\frac{\partial T}{\partial x} + T\frac{\partial(\kappa/\mu)}{\partial x}\right) \tag{16}$$

and

$$\beta_3(x,t) = R\left(\frac{\kappa}{\mu}\frac{\partial^2 T}{\partial x^2} + \frac{\partial T}{\partial x}\frac{\partial(\kappa/\mu)}{\partial x}\right) \tag{17}$$

The functions $\beta_1$, $\beta_2$, and $\beta_3$ can be considered to be known since $T(x,t)$, $V_b(x,t)$, and $\kappa(x,t)$ have been obtained above. The viscosity $\mu$ is also in general a function of temperature but it only varies by a factor of two over the temperature range under consideration and is thus taken as constant for the cases considered here.

Due to symmetry (Fig. 1), the boundary condition at the center of the body is

$$\text{at } x = 0, \quad \frac{\partial p}{\partial x} = 0 \tag{18}$$

The pressure at the outer edge of the body is assumed to be given by the pressure of the reactor $p_0$

$$\text{at } x = L, \quad p = p_0 \tag{19}$$

The initial pressure inside the body is also taken to be given by the reactor pressure:

$$\text{at } t = 0, \quad p = p_0 \tag{20}$$

To carry out these simulations, it is also required that a non-zero volume-fraction of gas be initially specified. In most cases, a value of $V_{g,0} = 10^{-3}$ was assumed, which is consistent with a very low value of initial porosity within the compact.

The above equations can be written in dimensionless form by defining $\rho = \frac{P_0}{RT_0}\bar{\rho}$.

Substitution of Eq. (13) for the permeability into Eq. (14) gives

$$\frac{\partial(V_g\bar{\rho})}{\partial\bar{t}} = \bar{\beta}_1\left[\bar{\rho}\frac{\partial^2\bar{\rho}}{\partial\bar{x}^2} + \left(\frac{\partial\bar{\rho}}{\partial\bar{x}}\right)^2\right] + \bar{\beta}_2\bar{\rho}\frac{\partial\bar{\rho}}{\partial\bar{x}} + \bar{\beta}_3\bar{\rho}^2 + \frac{\gamma RT_0 r(x,t)}{p_0 M} \tag{21}$$

where

$$\gamma = \left(\frac{\mu k S^2 L^2}{p_0}\right) \tag{22}$$

The parameter $\gamma$ – the gas flow time constant – can be considered to be proportional to the resistance to bulk flow. The dimensionless time is now defined to be $\bar{t} = t/\gamma$, and

$$\bar{\beta}_1 = \frac{T}{T_0}\frac{V_g^3}{(1-V_g)^2} \tag{23}$$

$$\bar{\beta}_2 = 3\frac{V_g^3}{(1-V_g)^2}\frac{\partial(T/T_0)}{\partial\bar{x}} + \frac{T}{T_0}\frac{\partial}{\partial\bar{x}}\left(\frac{V_g^3}{(1-V_g)^2}\right) \tag{24}$$

$$\bar{\beta}_3 = \frac{V_g^3}{(1-V_g)^2}\frac{\partial^2(T/T_0)}{\partial\bar{x}^2} + \frac{\partial(T/T_0)}{\partial\bar{x}}\frac{\partial}{\partial\bar{x}}\left(\frac{V_g^3}{(1-V_g)^2}\right) \tag{25}$$

The dimensionless Eqs. (21)–(25) for conservation of mass were solved by a well-established finite-difference method [20]. A Crank–Nicholson algorithm was employed for the time stepping [21].

## 3. Results and discussion

As is demonstrated by the formulation presented above, a model of the removal of binder from a ceramic green body requires consideration of many phenomena which necessarily involves a large number of parameters. To limit the scope of this paper, attention is focused primarily on the effects of heat and mass-transfer resistances on the buildup of pressure. These resistances are given by the heat-conduction time constant $L^2/\alpha$ and the time constant $\gamma$ associated with convective flow of binder decomposition products out of the body. Based on typical thicknesses and thermal diffusivities of ceramic green bodies, the range $10^3\ \text{s} \leq L^2/\alpha \leq 10^5\ \text{s}$ was explored. From typical values of the Kozeny–Carman parameters, gas viscosities, and body dimensions, the range $10^{-2}\ \text{s} \leq \gamma \leq 10^9$ was considered to be most relevant for the convective flow resistance. The parameters held constant in this work are given in Table 1.

### 3.1. Binder volume fraction

For the case of no heat and mass transfer resistance, the rate of binder decomposition $r$ and the change in binder volume fraction $V_b$ are shown in Fig. 3. For the case of zero-order kinetics, the reaction rate is slow at low temperatures and increases exponentially as a consequence of the Arrhenius dependence on temperature. The evolution of the volume fraction of binder is seen to be initially flat and then to drop sharply with increasing temperature. As a comparison, the case in which the binder decomposes according to first-order kinetics is also displayed. In this instance, the rate goes through a maximum, and the volume fraction of binder approaches zero, albeit more gradually. For example there is only a 10° difference in the temperature at which $V_b = 0.1$. For the purposes of this work in which we are determining how heat and mass transport phenomena influence the distribution of binder in the green body, the details of the kinetics are not crucial since all decomposition rates lead to decreases in $V_b$ as a function of temperature.

For a body with a finite thermal conductivity, the temperature is a function of position. The reaction rate and the volume fraction of binder are therefore, also functions of position. Fig. 4 shows the spatial variation of the reaction rate and binder volume fraction for various values of $T_L$, i.e., the temperature at the outer edge of the body. In this figure, $L^2/\alpha = 10^3$ s, which according to Eq. (7) corresponds to a temperature difference across the body of approximately 1°C. In this case, both the binder concentration and the reaction rate are uniform throughout the body for all temperature.

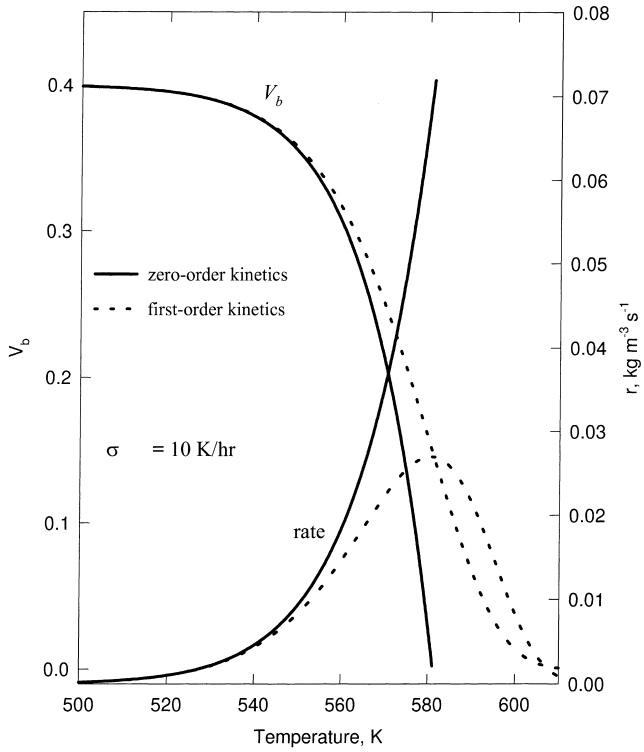


Fig. 3. The binder volume fraction $V_b$ and decomposition rate $r$ as a function of temperature for a linear heating rate with no heat and mass transfer resistances.

As seen in Fig. 5 for a body with a higher thermal resistance, i.e., when $L^2/\alpha = 10^4$ s, both binder distribution and the reaction rate within the green body become non-uniform. The fraction of binder at the edge of the body is lower than at the centerline, and the reaction rate exhibits a maximum. The abrupt decreases in the reaction rate observed for $T_L = 590$ and 585 K arise because binder is completely depleted at $x/L = 0.58$ and 0.83, respectively.

As is demonstrated in Fig. 6, the non-uniformity in decomposition kinetics and binder concentration become more pronounced for an even larger value of $L^2/\alpha$. In this instance, the distance over which the depletion of binder

Table 1
Parameters held constant in the simulations

| $T_0$ | $P_0$ | $V_s$ | $V_{b,0}$ | $\sigma$ | $\rho_b$ | $M$ | $k_0$ | $E_a$ |
|---|---|---|---|---|---|---|---|---|
| 300 K | 0.1 MPa | 0.6 | 0.399[a] | 0.0028° /s(10°/h)[b] | 1000 kg/m$^3$ | 40 g/mol | $3.87 \times 10^{14}$ kg/m$^3$/s | 175 kJ/mole |

[a] Except for the results shown in Fig. 12.
[b] Except for the results shown in Fig. 11.

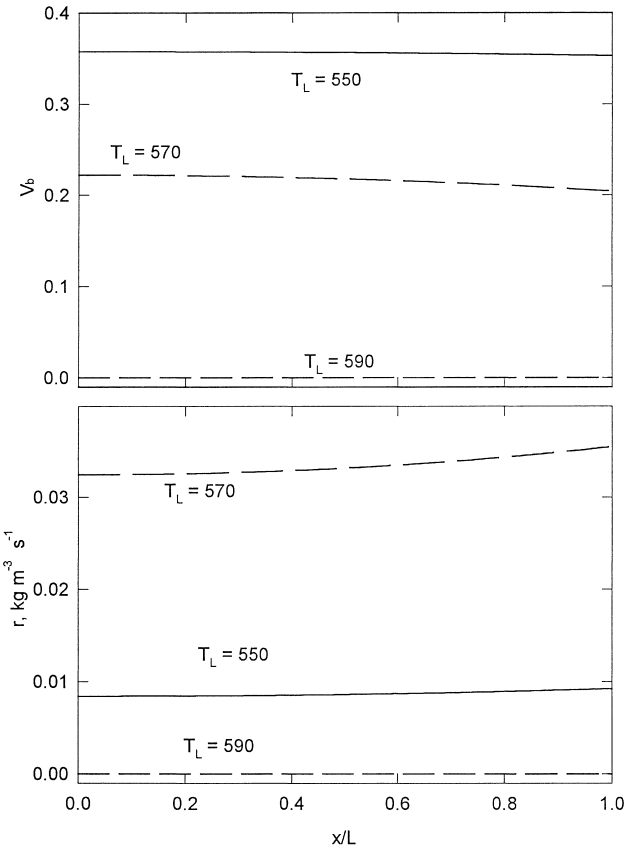


Fig. 4. The binder volume fraction $V_b$ (top panel) and the decomposition rate $r$ (bottom panel) as a function of position and edge temperature for $L^2/\alpha = 10^3$ s.

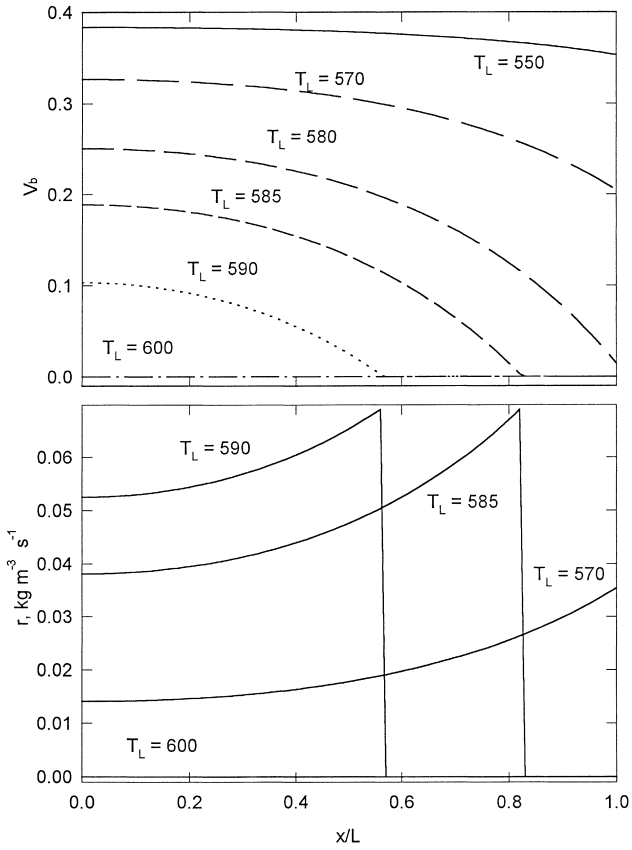


Fig. 5. The binder volume fraction $V_b$ (top panel) and the decomposition rate $r$ (bottom panel) as a function of position and edge temperature for $L^2/\alpha = 10^4$ s.

occurs becomes quite small. For $T_L = 690$ K, the outer 50% of the body is binder free, whereas the inner 25% contains more than 75% of its binder concentration. As before, the spatial locations corresponding to zero reaction rates are devoid of binder.

For most values of $T_L$ in Fig. 6, a sharp transition zone separates the body into regions which are binder free and binder rich. This situation is analogous to the assumption often made of planar binder removal, where it is proposed that binder decomposition occurs as a front which recedes into the body with increasing time. From these calculations we see, however, that removal of binder as a planar front is only realized when the heat-conduction time constant is large. For the smaller values of $L^2/\alpha$ represented by Figs. 4 and 5, sharp interfaces separating regions of the body with and without binder do not appear. In these latter two instances, the notion of binder removal proceeding as a planar front which recedes into the body is a poor representation of the physical phenomena.

Any number of alternative forms of the rate law for the decomposition kinetics as compared to Eq. (8) are also possible. The decomposition kinetics for most binders are measured by thermogravimetric analysis. Unless such experiments are conducted so as to eliminate heat and mass transfer resistances, such kinetics must be regarded as apparent and not true kinetics. This point is addressed more directly in the next section.

Nevertheless, the analysis conducted in this work indicates that for a given representation of the kinetics, mass and heat transfer effects can couple so as to give either planar or uniform distributions of binder within the green body.

### 3.2. Gas-flow and pressure buildup

The binder distribution profiles given in Figs. 4–6 arise as binder decomposes at faster rates at the elevated temperatures near the surface of the body. The temperature difference across the body can significantly affect the change in weight loss per unit volume, i.e., what is measured in a thermogravimetric experiment. This is demonstrated in Fig. 7, which shows that, as the heat-transfer resistance increases, the rate of weight loss per volume of the green body decreases. Larger values of the heat conduction time constant lead to slower apparent decomposition kinetics, even though the kinetics expression for the rate of decomposition was the same in all three simulations. This change in the apparent kinetics occurs as larger thermal resistance lead to a body which is cooler in the interior, and thus has a slower overall rate of weight loss.

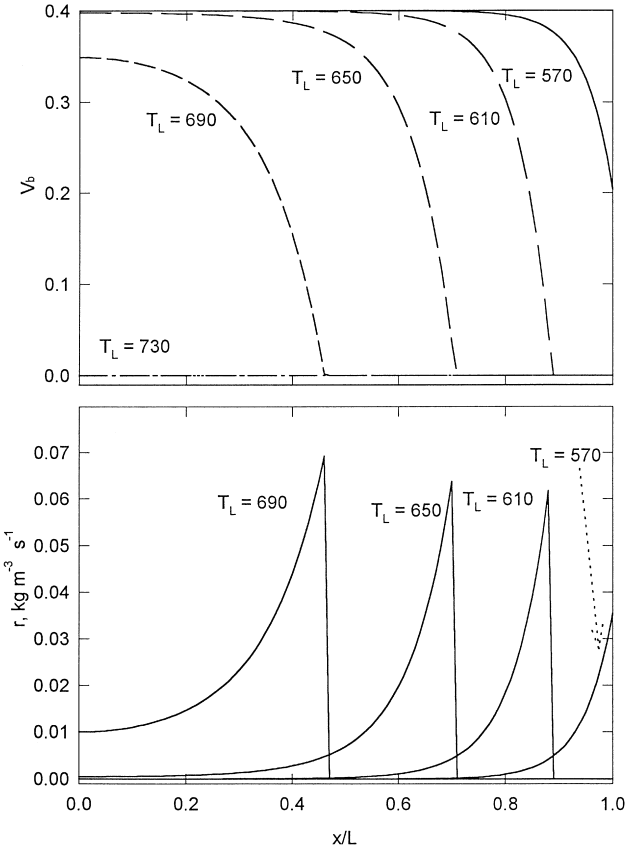


Fig. 6. The binder volume fraction $V_b$ (top panel) and the decomposition rate $r$ (bottom panel) as a function and edge temperature for $L^2/\alpha = 10^5$ s.

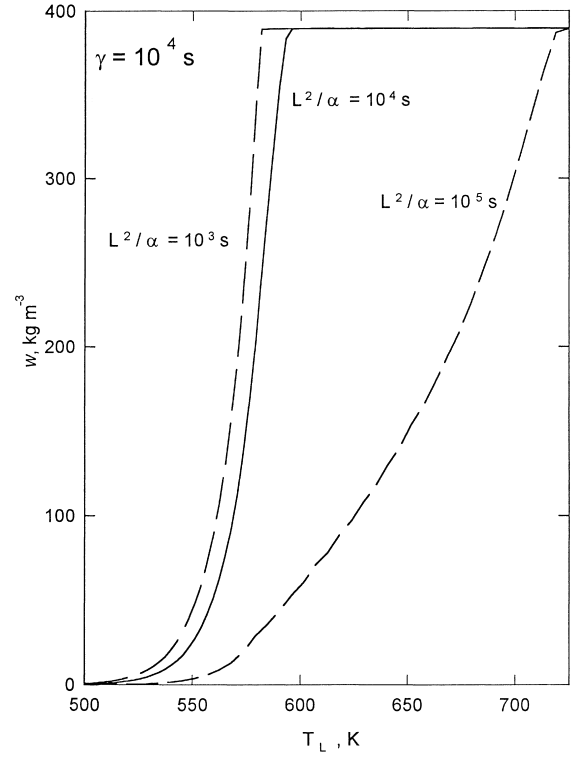


Fig. 7. The weight loss per volume vs. edge temperature for three values of the conduction time constant $L^2/\alpha$. The time constant $\gamma$ was set equal to $10^4$ s.

During binder removal, the presence of gas-phase decomposition products within the pore space of the body gives rise to pressure gradients and thus flow fields. The time constant for gas flow $\gamma$ is a measure of the time scale over which the bulk flow occurs. For the largest value of $\gamma$ – which represents the largest resistance to flow – the increase in pressure within the body will be at the most extreme. In Fig. 8(a–c) the dimensionless pressure distributions $P/P_0$ within the body are plotted for $\gamma = 10$ s and three values of the conduction time constant $L^2/\alpha$.

For the case of $L^2/\alpha = 10^3$ s in Fig. 8(a), relatively large variations in the dimensionless pressure are in evidence throughout the green body. The increase in pressure within the body is largest at intermediate temperatures when the binder decomposition rate begins to increase significantly, but the total binder content in the compact is still relatively high (see Fig. 4). The decrease in pressure ratio at higher temperatures, in spite of the more rapid decomposition kinetics, arises due to more rapid bulk flow throughout the binder-depleted and thus more porous body.

For the case of $L^2/\alpha = 10^4$ s in Fig. 8(b) – which corresponds to a larger temperature gradient within the body – the pressure distributions become more non-uniform. In fact, for the case $T_L = 550$, a pressure maximum is seen to occur near the outer edge of the body. As a consequence of this

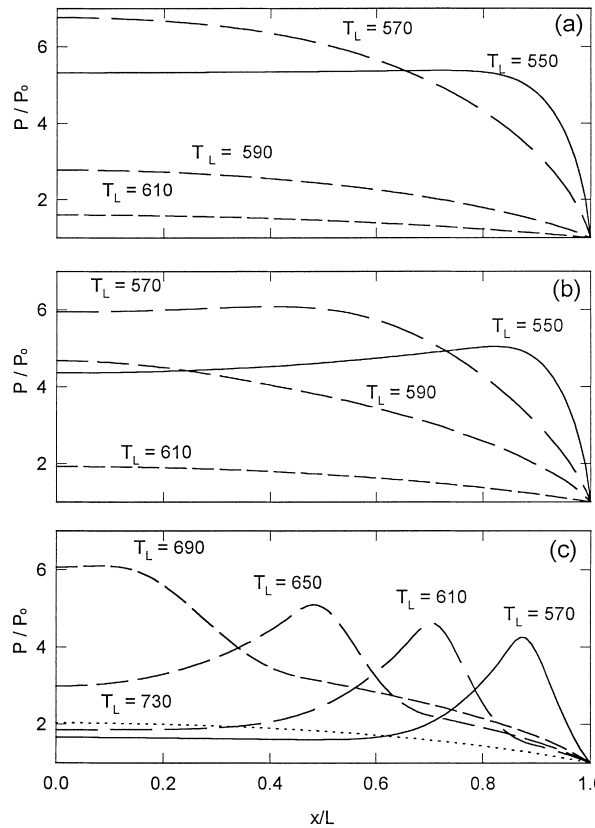


Fig. 8. The pressure ratio $P/P_0$ as a function of position and edge temperature for $\gamma = 10$ s and three values of $L^2/\alpha = 10^3$ s; (B) $L^2/\alpha = 10^4$ s; (C) $L^2/\alpha = 10^5$ s.

maximum, bulk flow of the binder decomposition products would occur in both directions in the body, although the majority of the flow would be outward as a result of the larger pressure gradient in this direction. It is interesting to note that the pressure at $T_L = 550$ obtains a maximum despite a nearly flat distribution of binder (see Fig. 5).

For the final case of $L^2/\alpha = 10^5$ s in Fig. 8(c), which corresponds to the largest temperature gradients within the body, the maximum in the pressure ratio arises more frequently throughout the heating ramp. In this instance, the bulk flow associated with the pressure gradient would be more substantial in both directions as compared to the conditions in Fig. 8(b).

The physical explanation for the origin of a maximum in the pressure can be understood readily. As seen upon comparison of the binder and reaction rate profiles from Fig. 6 with pressure profiles in Fig. 8(c), the location of the pressure maximum is slightly deeper into the body than the sharp fronts associated with the decrease in binder content and decomposition rate. From the location of these fronts outward, there is no residual binder left in the body, bulk flow is rapid in the open pore space, and the pressure remains low. Inward from the position of the fronts, however, the temperature is lower as a consequence of the large thermal resistance, and the evolution of gas-phase decomposition products – and therefore, the pressure – is low. In conclusion, the occurrence of a maximum in the pressure with the body is a direct consequence of the coupling between the heat and mass transfer resistances.

As suggested by the figures, the absolute maximum in the pressure ratio occurs at the centerline of the body, and thus, the maximum stress is associated with the pressure increase at this location. Simulation results for two conduction time constants and various flow time constants $\gamma$ have been therefore, summarized in Fig. 9 to indicate the progression of $P_{center}/P_0$ as the temperature is increased.

For a given value of $\gamma$, $P_{center}/P_0$ is unity at low temperature where binder decomposition is negligible. As the temperature is increased, the pressure ratio increases as a consequence of accelerated decomposition kinetics. With further increasing temperature, the decrease in $P_{center}/P_0$ arises from enhanced bulk flow through the more porous body and ultimately from the extinguishing of the reaction as binder is consumed. In general, $P_{center}/P_0$ depends strongly on the time constant for gas flow $\gamma$. The effect of increasing $L^2/\alpha$ is to shift the maximum in $P_{center}/P_0$ to higher values of $T_L$, but it was found to have a relatively smaller impact on the maximum value of $P_{center}/P_0$.

The most important insight provided by the simulations is that the magnitude of $P_{center}/P_0$ can be large. For $P_0 = 0.1$ MPa, the pressure can be approximately 0.7 Mpa. Since the green strength of a fully debinderized body is typically 0.2–0.5 Mpa, failure of the ceramic body can occur. This is especially pronounced for bodies with high values of $\gamma$, i.e., high green densities, where the resistance to bulk flow is large.

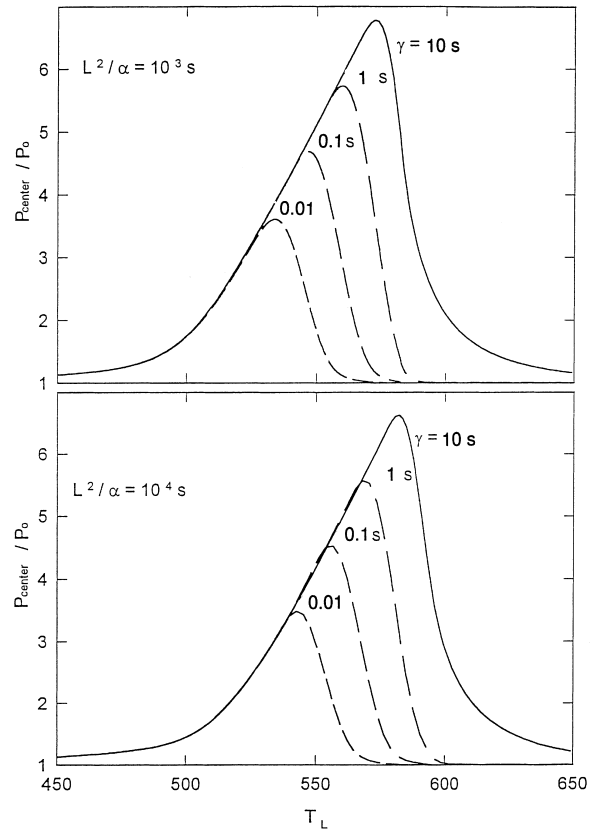


Fig. 9. The pressure ratio $P_{center}/P_0$ vs. edge temperature for selected values of the constant for bulk flow $\gamma$ and the conduction time constant $L^2/\alpha$.

A more concise summary of the simulations is to show the maximum in the centerline pressure ratio $P_{max}/P_0$ in the body as a function of $\gamma$ for various values of $L^2/\alpha$. As seen in Fig. 10, the pressure ratio depends logarithmically on $\gamma$ with a weaker dependence on $L^2/\alpha$. The data of Fig. 10 are consistent with the well-established notion that is more difficult to remove binder as the thickness of the body increases. For example, a body of thickness $L$ whose thermal characteristics are such that it is located at point A would realize a maximum pressure increase of 4.57 at the centerline. Increasing the thickness by a factor of 10 results in a 100-fold increase in both the thermal resistance and the resistance to bulk flow. The maximum pressure associated with this thicker body – denoted by point B in Fig. 10 – is 6.4, and this body therefore, would be more susceptible to failure from fracture.

In all of the above simulations, the temperature ramp rate was taken to be 10 K/h. Since the ramp rate is the parameter most often varied to optimize binder burnout, it is interesting to investigate its effect. In Fig. 11, the normalized centerline pressure is plotted as a function of $T_L$ for three ramp rates. As the ramp rate decreases, the maximum pressure in the green body decreases which is in accord with the physical expectation.

The sensitivity of the pressure buildup, as given by $P_{center}/P_0$, as a function of the initial volume fraction of the gas in

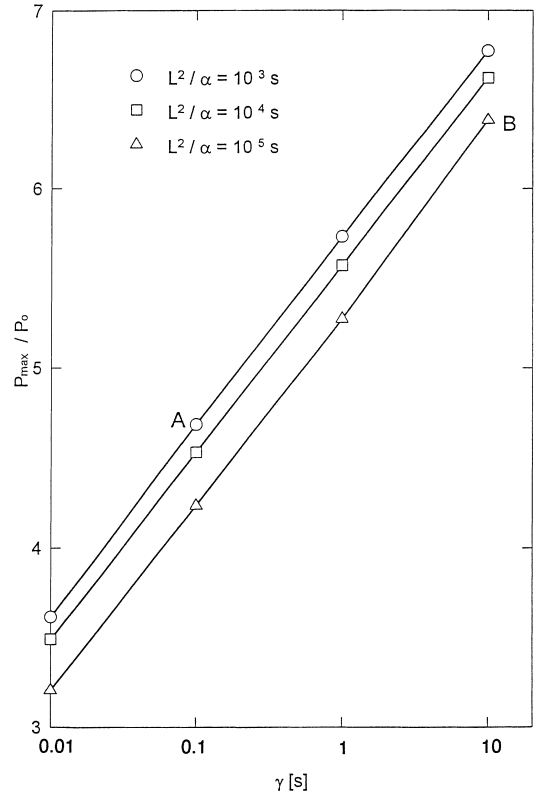


Fig. 10. The maximum pressure ratio vs. the time constant for bulk flow $\gamma$ for three values of $L^2/\alpha$.

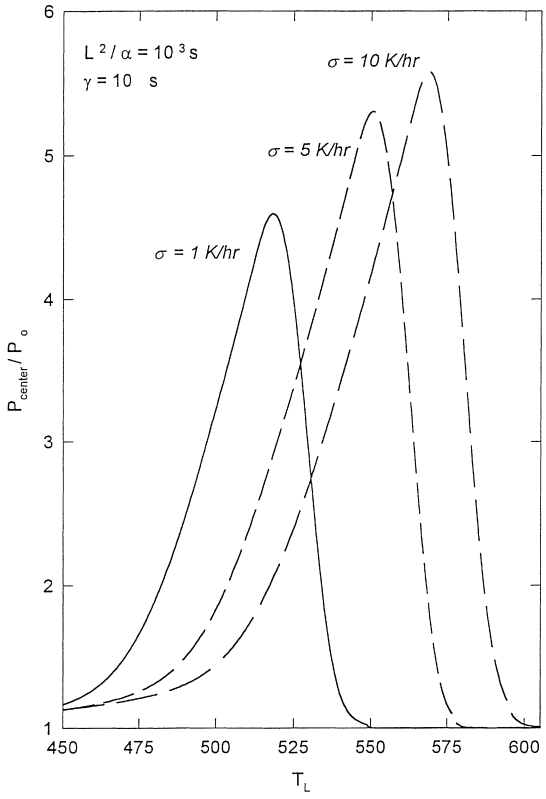


Fig. 11. The pressure ratio $P_{center}/P_0$ as a function of edge temperature for three values of the furnace-temperature ramp rate. In this figure, $L^2/\alpha = 10^4$ s and $\gamma = 10^3$ s.

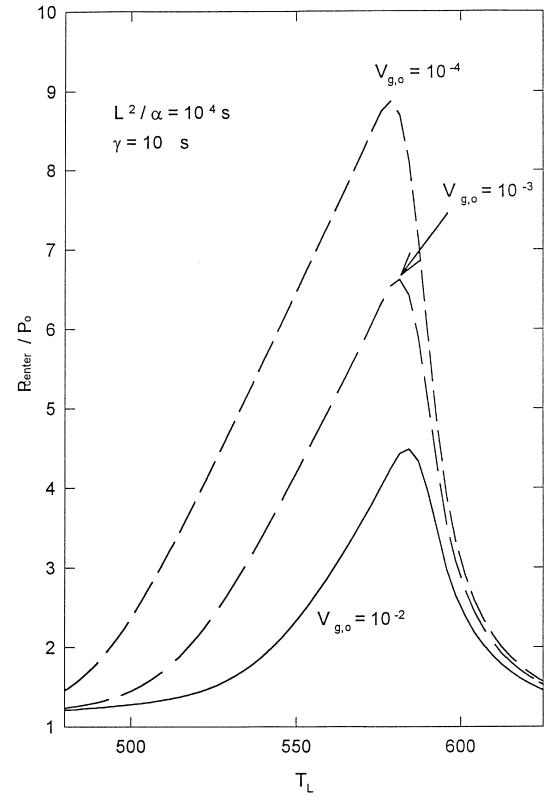


Fig. 12. The sensitivity of the pressure ratio $P_{center}/P_0$ to the value of the initial porosity $V_{g,0}$.

the green body is given by Fig. 12. The pressure ratio $P_{center}/P_0$ decreases dramatically when more porosity is present at $t = 0$. This illustrates that the presence of even low levels of interconnected porosity during the initial stages of binder decomposition can serve as a powerful method to mitigate the effects of pressure buildup during binder removal.

## 4. Conclusions

A mathematical model has been developed to describe of binder from injection-molded ceramic components. The model takes into account the effects of heat transfer, mass transfer, and reaction kinetics within the ceramic body. The temperature, porosity, and pressure profiles within the body and their temporal evolution are obtained from the numerical solution of the governing equations.

The temperature, porosity, and pressure profiles show a number of interesting trends. For large values of the thermal and flow resistances, non-uniformities in the temperature, binder concentration, and pressure can arise within the body. In the most extreme cases, a maximum in the pressure profile can arise.

The evolution of the binder distribution within the green body as a function of time shows two types of behavior. In one case, the removal of binder as a planar front which recedes into the body with time occurs. However, these

types of binder profiles only arise for large values of the heat conduction and convective flow resistances. For smaller values of these two parameters, removal of binder proceeds uniformly throughout the body. Thus, the model is able to aid in estimating which types of furnacing conditions will lead to minimum gradients in the binder distribution.

The most useful insight provided by the model is the magnitude of the increases in pressure which may occur during binder burnout. As expected, fast heating rates and large resistances to bulk flow exacerbate this effect. The magnitude of the pressure increase can approach seven times atmospheric pressure, and the stresses associated with this is sufficient in many instances to lead to fracture of the green body. In addition, the model is able to show how low levels of interconnected porosity present during the initial stages of binder removal can have a substantial impact on facilitating convective flow within the body and thus reduce the buildup of pressure.

## 5. Nomenclature

| | |
|---|---|
| $E_a$ | activation energy, J/mol |
| $k$ | Kozeny–Carman parameter |
| $K_0$ | reaction rate constant, kg/m$^3$/s |
| $L$ | half-thickness of green body, m |
| $p$ | pressure, Pa |
| $p_0$ | pressure of reactor, Pa |
| $R$ | gas constant, 8.314 J/mol/K |
| $S$ | specific surface area, m$^{-1}$ |
| $t$ | time, s |
| $\bar{t}$ | dimensionless time (based on gas-flow time constant) |
| $T$ | temperature, K |
| $T_L$ | temperature at body edge ($x = L$), K |
| $T_0$ | initial temperature, K |
| $u$ | gas velocity, m/s |
| $V_b$, $V_g$, $V_s$ | volume fractions of binder, gas, and solid |
| $w$ | weight loss per unit volume, kg/m$^3$ |
| $\alpha$ | thermal diffusivity, m$^2$/s |
| $\beta_1$, $\beta_2$, $\beta_3$ | functions defined by Eqs. (15)–(17) |
| $\bar{\beta}_1, \bar{\beta}_2, \bar{\beta}_3$ | dimensionless functions defined by Eqs. (23)–(25). |
| $\gamma$ | gas flow time constant, s |
| $\kappa$ | gas permeability, m$^2$ |
| $\mu$ | gas viscosity, Pa s |
| $\rho$ | gas density, mol/m$^3$ |
| $\bar{\rho}$ | dimensionless gas density |
| $\rho_b$ | binder density, kg/m$^3$ |
| $\Theta$ | dimensionless temperature |
| $\sigma$ | temperature ramp rate, K/s |
| $\tau$ | dimensionless time based on conduction time constant |

## References


[1] B.C. Mutsuddy, Injection molding, in: S.J. Schneider (Ed.), Engineered Materials Handbook, Ceramics and Glasses, vol. 4., Materials Information Society, 1991, pp. 173–180.

[2] B.C. Mutsuddy, Injection molding research paves the way to ceramic engine parts, J. Ind. Res. Dev. 25 (1983) 76–80.

[3] G. Bandyopadhyay, K.W. French, Injection-molded ceramics: critical aspects of the binder removal process and component fabrication, J. Eur. Ceram. Soc. 11 (1993) 23–34.

[4] R.M. German, Theory of thermal debinding, Int. J. Powder Metall. 23(4) (1987) 237–245.

[5] P. Calvert, M. Cima, Theoretical models for binder burnout, J. Am. Ceram. Soc. 73(3) (1990) 575–579.

[6] M.J. Cima, J.A. Lewis, A.D. Devoe, Binder distribution in ceramic greenware during thermolysis, J. Am. Ceram. Soc. 72(7) (1989) 1192–1199.

[7] M.R. Barone, J.C. Ulicny, R.R. Hengst, J.P. Pollinger, Removal of organic binders in ceramic powder compacts, in: G.L. Messing, E.R. Fuller, Jr., H. Hausnerpp, Ceramic Transactions. vol. 1A, Ceramic Powder Science II, American Ceramic Society, Westerville, OH, 1988, pp. 575–583.

[8] M.R. Barone, J.C. Ulicny, Liquid-phase transport during removal of organic binders in injection-molded ceramics, J. Am. Ceram. Soc. 73(11) (1990) 3323–3333.

[9] D.-S. Tsai, Pressure buildup and internal stresses during binder burnout: numerical analysis, AIChE J. 37(4) (1991) 547–554.

[10] A. Manguin-Fritsch, H. Burlet, P.M. Fourt, M. Abouaf, Modélisation de la Pyrolyse d'un Liant Organique de Mise en Forme de Pièces Céramiques Injectées, L'Industrie Céramique and Verrière 887 (1992) 744–749.

[11] B.K. Lograsso, R.M. German, Thermal debinding of injection molded powder compacts, Powder Metallurgy Int. 22(1) (1990) 17–22.

[12] G.W. Sherer, Theory of drying, J. Am. Ceram. Soc. 73(1) (1990) 3–14.

[13] W.L. McCabe, J.C. Smith, Unit Operations of Chemical Engineering, McGraw-Hill, New York, 1976.

[14] R.B. Bird, W.E. Stewart, E.N. Lightfoot, Transport Phenomena, Wiley, New York, 1960.

[15] G.C. Stangle, I.A. Aksay, Simultaneous momentum, heat and mass transfer with chemical reaction in disordered porous medium: application to binder removal from a ceramic green body, Chem. Eng. Sci. 45 (1990) 1719–1733.

[16] L.J. Klinkenberg, The permeability of porous media to liquids and gases, Drill. Proc. Proc. API (1941) 200–213.

[17] H.S. Carlslaw, J.C. Jaeger, Conduction of Heat in Solids, 2nd ed., Oxford University Press, Oxford, 1959.

[18] I.A. Aksay, C.H. Schilling, Mechanics of Colloidal Filtration, in: J.A. Mangels, G.L. Messing, Advances in Ceramics: Forming of Ceramics, vol. 9, American Ceramic Society, Columbus, OH, 1984, pp. 85–93.

[19] J.F.K. Kotte, J.A.M. Denissen, R. Metselaar, Pressure casting of silicon nitride, J. Eur. Ceram. Soc. 7 (1991) 307–314.

[20] J. Newman, Numerical solution of coupled, ordinary differential equations, Ind. Eng. Chem. Fund. 7 (1968) 515–517.

[21] W.H. Press, B.P. Flannery, S.A. Teukolsky, W.T. Vetterling, Numerical Recipes, The Art of Scientific Computing, Cambridge University Press, Cambridge, 1989.